Silica supported Sn catalysts with tetrahedral Sn sites for selective isomerization of glucose to fructose

Yayati Naresh Palai,[a,b] *Abhijit Shrotri,*[a]* *Miyuki Asakawa,*[a,b] *Atsushi Fukuoka*[a]*

[a]Institute for Catalysis, Hokkaido University, Kita 21 Nishi 10, Kita-ku, Sapporo, Hokkaido 001-0021, Japan

[b]Graduate School of Chemical Sciences and Engineering, Hokkaido University, Kita 13 Nishi 8, Kita-ku, Sapporo, Hokkaido 060-8628, Japan

Abstract

Lewis acid catalyzed isomerization of glucose to fructose is an important reaction for production of renewable chemicals. Here, we show the synthesis of an active and selective Lewis acid catalyst for this reaction by controlling Sn dispersion on SBA15. Sn loading of 1 wt. % over SBA15 (Sn/SBA15) maximized the formation of tetrahedral Sn species on the catalyst surface. Increasing the loading or changing support caused formation of SnO_2 clusters which reduced fructose selectivity. A mechanism based on condensation of Sn with silanol group of SBA15 is proposed. The catalyst showed high selectivity of 93 % after 2 h with 57 % fructose yield. The Lewis acid catalyzed isomerization of glucose was proven by isotopic tracer study using D-glucose-2-d. The catalyst deactivated in the third cycle owing to byproduct deposition, but the activity was restored by recalcining the catalyst.

Graphical abstract

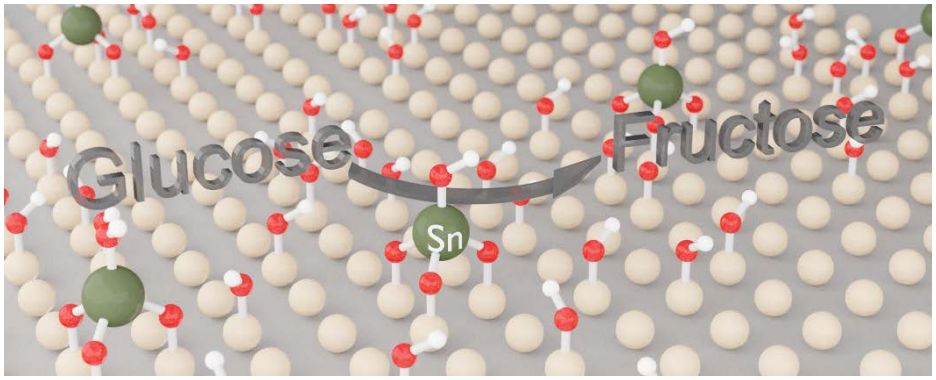

Keywords

Glucose isomerization, Lewis acidity, Tin catalyst, Fructose, SBA15

1. Introduction

Cellulose depolymerization to glucose and its subsequent isomerization to fructose is the gateway to many industrially important chemicals [1–3]. Isomerization of glucose to fructose converts the aldohexose sugar to its ketohexose form. The ketohexose fructose conforms to furanose ring structure in a solution, which enables the synthesis of 5-hydroxymethyl furfural (5-HMF) [4], a precursor for bio-based plastics [5,6]. Fructose is also the major component of high fructose corn syrup, an industrial sweetener, derived from corn starch [7]. Therefore, the isomerization of glucose to the less abundant fructose is an important reaction in food and chemical industries.

Industrial process for glucose isomerization utilizes immobilized xylose isomerase as a catalyst [8]. This enzyme can selectively catalyze glucose isomerization to fructose. However, issues associated with high processing cost, low lifetime of enzyme and requirement of a buffer to maintain the pH of reaction medium increase the process cost.

Histidine groups present in the enzyme structure were initially thought to be the active sites for glucose isomerization [9]. Later it was found that the metal center has an essential role in stabilizing the acyclic glucose molecule and the subsequent isomerization reaction [10–12]. Since then, several reports on base or Lewis acid catalyzed reactions have appeared for glucose isomerization

Base catalyzed isomerization of glucose proceeds via the Lorry de Bruyn-Alberda van Ekenstein transformation of glucose initiated by proton abstraction at the C2 position [13]. Recently

our group reported a hydrotalcite catalyst containing basic sites that achieved 56 % yield of fructose with 80% selectivity [14]. Use of ethanol as solvent shifted the equilibrium towards fructose in this reaction. Other examples include SBA15 grafted with tertiary amine groups acting as base catalysts that achieved 41 % fructose yield with 85 % selectivity [15]. Zhang et al. reported a series of imidazolium and tertiary amine based ionic liquids that serve as base catalysts for this reaction [16]. Several other base catalysts have been reported for glucose to fructose reactions [17–21]. However, the inadequate stability of these basic catalysts is still a hinderance for industrial application.

Corma et al. first showed that Sn-Beta zeolites with Lewis acid sites can do the Meerwein–Ponndorf–Verley (MPV) reduction of carbonyl compounds via hydride shift from a neighboring hydroxyl group to the carbonyl group [22]. Glucose to fructose isomerization over Lewis acid catalysts can be explained by a similar mechanism where the C2 carbon donates a hydride ion to the C1 aldehyde group which leads to the formation of a ketone group at the C2 position [13]. Sn and Ti incorporated porous materials have been reported to facilitate this reaction with high yield [13,23–26]. Sn-Beta catalyzes isomerization of glucose, xylose and dihydroxyacetone, whereas Sn-MFI only catalyzes the isomerization of xylose and dihydroxyacetone. The larger pore size of Sn-Beta in comparison to Sn-MFI facilitated diffusion of the relatively bulkier glucose molecule within its pores [27]. Spectroscopic analysis has revealed that tetrahedral Sn open sites within the pores, containing three Si-O-Sn bonds and one Sn-OH bond, are most active for isomerization reaction [26]. Sn-Beta catalyst has received much attention over the years for this reaction. The reaction mechanism has been confirmed with experimental data [13], and theoretical modelling has shown that 1,2-hydride shift is the rate determining step [28]. However, practical application of this catalyst has been hindered owing to the cumbersome method for synthesis of Sn-Beta zeolite and its deactivation.

Sn containing mesoporous materials such as Sn/SBA15 and Sn/MCM41 are alternative to zeolite-based catalysts. Lorenti et al. reported a series of Sn-SBA-15 materials for glucose to fructose isomerization with 11.8 % glucose conversion and 84.5 % selectivity [29]. Apart from glucose isomerization, Sn containing mesoporous silica catalysts have also found application in Bayer-Villiger oxidation of adamantanone [30,31].

Sn on mesoporous supports can exhibit both Lewis acidity and basicity owing to the formation of tetrahedral Sn-OH species and bulk SnO_2 respectively. Deval et al. showed that both these sites can show activity for glucose isomerization in the presence of an organic solvent [26]. Although Lewis acid sites show higher activity and selectivity towards the isomerization reaction, it is difficult to control the formation of Lewis acid sites on mesoporous materials as the Sn particle easily agglomerate to form SnO_2 species.

In this work, we explore the synthesis of highly active Sn based catalyst with tetrahedral Lewis acid sites on mesoporous silica and other oxide supports and investigate the catalytic activity for glucose isomerization in ethanol along with detailed characterization to correlate the formation of active sites with fructose yield and selectivity.

2. Experimental

2.1 Materials

All materials and reagents used in this study are commercially available. Glucose and fructose were purchased from Wako Chemicals. D-Glucose-2-d and $SnCl_4 \cdot 5H_2O$ were purchased from Sigma Aldrich. Tetraethyl orthosilicate was bought from TCI Chemicals. H-Beta150 (Beta zeolite with SiO_2/Al_2O_3 ratio of 150) and zirconia were obtained from Japan Reference Catalysts (JRC). Titania (MC-150) was obtained from Ishihara Sangyo, Japan. γ-Alumina was bought from Sigma Aldrich.

2.2 Catalyst preparation

SBA15 was prepared according to a method reported by Stucky et al. [32]. During synthesis, 450 mL of 1.6 M hydrochloric acid was added to 12 g of poly(ethylene glycol)-block-poly(propylene glycol)-block-poly(ethylene glycol) (P123) and stirred at room temperature until the P123 was hydrolyzed. The solution was stirred rapidly at 35 °C and 25.5 g of tetraethyl orthosilicate was added dropwise over a span of 30 minutes. The solution was kept standing at 35 °C for 24 h and further at 100 °C for another 24 h. The obtained solid was filtered and washed with water and ethanol until the presence of chloride ions was not detected in the filtrate. The solid was dried at 110 °C overnight and then calcined at 560 °C for 16 h to obtain SBA15.

Sn containing catalysts were prepared by impregnation method. Desired amount of

$SnCl_4.5H2O$, was dissolved in 5 mL of distilled water and then 500 mg of support was added to the solution. The mixture was sonicated for 5 minutes and then stirred continuously with a glass rod over a hot plate maintained at 110 °C until a powder was obtained. After further drying at 110 °C for 2 h, the powder was calcined at 500 °C for 2 h.

2.3 Catalyst characterization

X-ray diffraction (XRD) was measured with Rigaku MiniFlex using CuKα X-ray (λ = 1.54 Å) operating at 40 kV and 20 mA. UV visible diffuse reflectance spectroscopy (UV-vis) measurement was obtained using Jasco V-650 spectrophotometer, line width of light ray was kept at 1 nm and $BaSO_4$ was used as reference. N_2 adsorption isotherms were measured at −196 °C using a Belsorp mini analyzer. Surface area was calculated by using BET theory between the relative pressure range 0.05 to 0.35 in the N_2 adsorption isotherm.[33] STEM image was obtained in a JEOL JEM-ARM200F atomic resolution electron microscope at an acceleration voltage of 200 kV equipped with and EDS detector EX-24221M1G5T. X-ray photoelectron spectroscopy (XPS) was performed with JEOL JPS-9010MC instrument. Charge correction was made by adjusting the adventitious carbon peak to 286.4 eV. Pyridine IR spectrum was recorded in a Shimadzu IRSpirit instrument. The samples were pressed into self-supported disks and placed in a quartz cell inside a high vacuum chamber with NaCl windows. The sample was pretreated under high vacuum at 150 °C for 1 h, before recording any spectrum in order to remove physisorbed moisture. Energy dispersive X-ray spectroscopy (EDX) analysis of reaction solution was done with Shimadzu Edx – 720 instrument.

2.4 Catalytic experiments

Catalytic glucose isomerization was performed in a 15 mL high pressure glass tube. In a typical reaction 90 mg glucose, 90 mg catalyst, 7 mL ethanol was taken in the high-pressure tube, which was then heated at 90 °C in an oil bath, with magnetic stirring. After the reaction was complete the mixture was centrifuged to separate the catalyst and the solution. Additionally, the catalyst was washed with deionized water (2 ml × 3 times) to extract physically adsorbed reactant and product species. The wash off water was mixed together with the reaction mixture and analyzed with a HPLC system equipped with Shodex SH1011 sugar column. Conversion and yield were calculated with an

absolute calibration using the formulae:

$$\text{Conversion} = \frac{moles\ of\ glucose\ remaining}{moles\ of\ glucose\ taken} \times 100$$

$$\text{Fructose yield} = \frac{moles\ of\ fructose\ formed}{moles\ of\ glucose\ taken} \times 100$$

$$\text{Selectivity} = \frac{fructose\ yield}{conversion} \times 100$$

$$\text{TOF} = \frac{number\ of\ moles\ of\ fructose\ formed}{number\ moles\ of\ metal\ \times\ reaction\ time}$$

The isotope tracer study was done using D-glucose-2-d as the reactant and adding sodium acetate-d_3 as an internal standard after the isomerization reaction. The final reaction mixture was analyzed by ^{2}H nuclear magnetic resonance spectroscopy (NMR; JEOL, JNM- ECX600, 2H 92.1 MHz).

3. Results and discussion

3.1 Catalytic activity

Sn containing catalyst were prepared by impregnating Sn (1 wt. %) on supports such as SBA15, H-Beta150 zeolite, A380 silica, alumina, zirconia and titania. All catalysts were tested for isomerization of glucose to fructose at 90 °C in the presence of ethanol as the solvent with a glucose concentration of 1.6 wt. % (glucose to Sn ratio = 66). Ethanol was chosen as the solvent because it can be easily obtained from renewable biomass and it shows high fructose selectivity among polar organic solvents [14,34]. Sn/SBA15 showed the highest fructose selectivity of 98 % along with 38 % conversion after 45 min of reaction (Fig. 1a). Sn/H-Beta150 showed slightly higher conversion (44 %) than Sn/SBA15 with a lower selectivity of 89 %. Beta zeolites are known to exhibit Brønsted acid sites originating from the presence of Al atoms in the framework resulting in unwanted side reactions. A small amount (less than 1 %) of 5-HMF was detected in this reaction which is formed by dehydration of fructose over Brønsted acid sites [35–39]. Formation of 5-HMF also results in humin production, a polymer of 5-HMF and other products, which is likely to reduce the selectivity towards fructose in the

presence of Sn/HBeta150. Sn/A380 showed comparable selectivity towards fructose (90 %), although the conversion was markedly lower (24 %). Sn/Zirconia showed no activity for fructose formation. Titania and alumina based catalysts showed some activity ca. 64 % selectivity at 10 % conversion and 77 % selectivity at 16 % conversion, respectively. Overall, silica-based supports showed better activity and selectivity than other oxide supports. In particular, SBA15 showed the highest selectivity with comparatively high conversion.

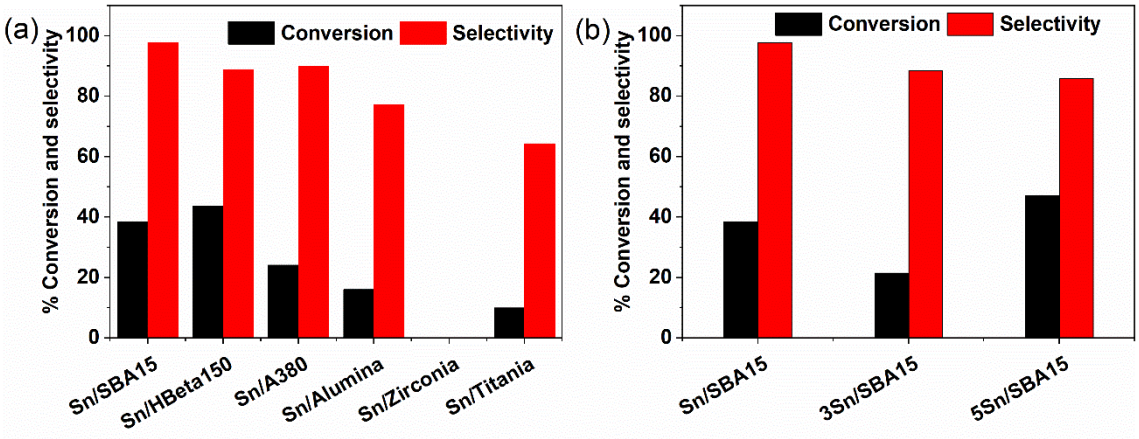

Fig. 1. Fructose selectivity and glucose conversion in the presence of (a)1 wt. % Sn catalyst using different supports and (b) catalyst with different Sn loading over SBA15. Reaction conditions: 90 mg glucose, 90 mg catalyst, 7 mL ethanol, 90 °C, 45 minutes.

Next, we investigated the role of Sn loading over SBA15. Increasing the Sn content to 3 wt. % (3Sn/SBA15) reduced the selectivity to 89 % and also decreased the glucose conversion to 21 % (Fig. 1b). Further increase in Sn loading to 5 wt. % (5Sn/SBA15) did not enhance the fructose selectivity (86 %). However, the glucose conversion increased to 47%. In this reaction, less than 1 % 5-HMF was observed, however the reaction mixture turned slightly yellow indicating the formation of soluble humins.

Based on the above results Sn/SBA15 with 1 wt. % Sn loading was chosen for optimization of reaction condition. Fructose selectivity of 99 % was obtained in the initial stage of reaction (30 min), which reduced slightly to 93 % after 2h. (Fig. 2) Glucose conversion increased steadily to 62 % until 2 h resulting in 57 % fructose yield. At this time the reaction reached equilibrium and further prolonging the time to 3 h increased the fructose yield to 60 % along with a reduction in selectivity to 85 % owing to byproduct formation. Increasing the glucose concentration to 10 % w/w (glucose to Sn

ratio = 462) under the same reaction condition resulted in 34 % yield with 79 % selectivity for fructose after 2 h of reaction. The turnover frequency in this reaction at 45 min was 53.6×10^{-3} s^{-1}, (based on molar content of Sn), which is higher than the previously reported value of 27.8×10^{-3} s^{-1} for Sn-Beta catalyst in water [26].

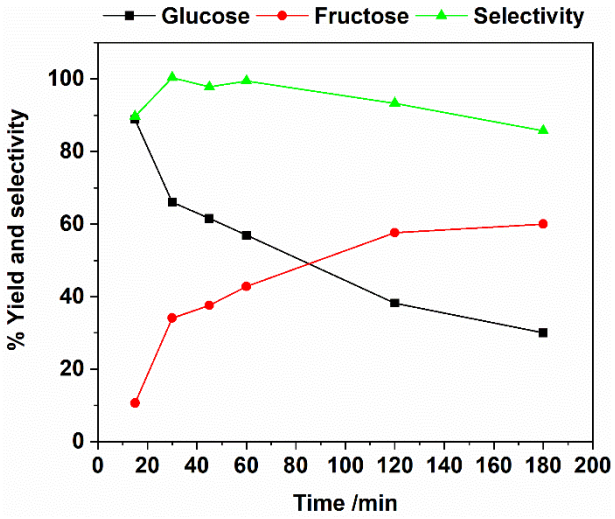

Fig. 2. Reaction time course using Sn/SBA15 catalyst (1 wt. % Sn). Reaction conditions: 90 mg glucose, 90 mg catalyst, 7 mL ethanol, 90 °C.

3.2 Catalyst characterization

All catalysts were characterized to investigate the underlying factors responsible for change in fructose selectivity and yield with the change in catalyst support and Sn loading. The XRD pattern for 5Sn/SBA15 (Fig. 3), having the highest Sn loading, showed characteristic peaks for cassiterite SnO_2 (PDF card number 01-077-0449). The crystallite size for SnO_2 was calculated as 13.7 nm suggesting formation of large SnO_2 particles, which might contribute towards the poor selectivity for this catalyst. In case of 3Sn/SBA15 only the prominent peaks at 2θ value of 26.6, 33.8, 37.9 and 51.7 degrees were observed. The crystallite size was determined as 3.7 nm, which suggested formation of smaller SnO_2 particles at lower loading. The XRD pattern for Sn/SBA15 was exactly similar to unsupported SBA15 and no peaks for SnO_2 were observed. This indicates that reducing the amount of Sn species on the surface increased the Sn dispersion and reduced the formation of SnO_2 clusters. It is reported that the SnO_2 phase does not exhibit the Lewis acid sites required for glucose isomerization and formation of tetrahedral Sn species is needed to achieve high activity. SnO_2 peaks were not

observed on other support as well when the Sn loading was 1% (Fig. S1) suggesting high dispersion of Sn species at low loading irrespective of the type of support used.

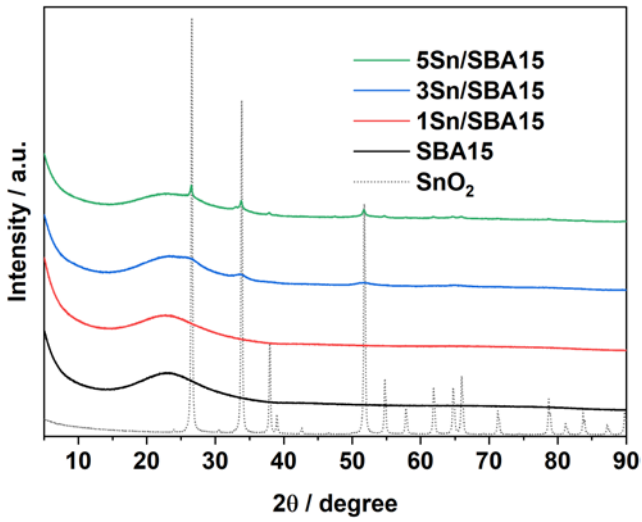

Fig. 3. XRD pattern of Sn/SBA15 catalysts with different Sn loading

UV-Visible spectroscopy of Sn catalysts on silica-based supports was performed in the diffuse reflectance mode to further elucidate the nature of Sn species on the catalyst (Fig. 4). The region below 210 nm in the spectrum is a result of reflectance from the tetrahedrally coordinated Sn species responsible for high activity.[26] Reflectance in this region was 33 % for Sn/SBA15, 31% for 3Sn/SBA15 and 27 % for 5Sn/SBA15 indicating that all catalysts contained Sn species with tetrahedral coordination. The region close to 280 nm can be assigned to hexacoordinated Sn species present within the SnO_2 crystal. Furthermore, the reflectance close to 250 nm is a result of LMCT charge transfer due to interaction of tetrahedrally coordinated Sn species with other basic oxygen and nitrogen containing compounds. Reflectance around 280 nm for Sn/SBA15 was close to baseline, whereas 52% reflectance was observed in case of 3Sn/SBA15 and 43 % in case of 5Sn/SBA15, indicating formation of inactive hexacoordinated Sn species with an increase in Sn loading. Reflectance around 250 nm for Sn/SBA15 was attributed to interaction of tetrahedrally coordinated Sn species with physisorbed water within the pores of SBA15. Similarly, for 3Sn/SBA15 and 5Sn/SBA15, reflectance in this region was assigned to interaction of tetrahedrally coordinated Sn species with physisorbed water and nearby basic SnO_2 species. However, in this case some contribution from blue shifting of ~280 nm band to ~250 nm due to small particle size of the SnO_2 is also likely [40–43].

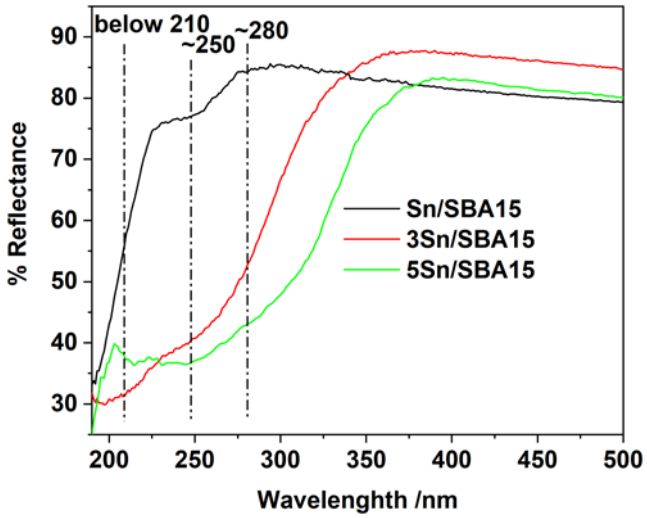

Fig. 4. DRUV-VIS spectra of Sn/SBA15 with different metal content

The effect of different silica support with the same Sn loading on Sn species are compared in Fig. 5. The reflectance owing to tetrahedrally coordinated Sn centers in Sn/A380 catalyst was similar to that of Sn/SBA15, 37% and 33% respectively. However, Sn/A380 also showed reflectance in the 280 nm and 250 nm region, which was attributed to the lower surface area of A380 silica gel (300 m^2 g^{-1}) in comparison to SBA15 (850 m^2 g^{-1}) (Table S1), resulting in poorer dispersion of Sn species at similar metal loading. The Sn/HBeta150 catalyst showed moderate reflectance in the 210 nm region. Reflectance in the 280 nm and 250 nm regions were also observed, which were attributed to formation of small SnO_2 clusters within the micropores of zeolite.

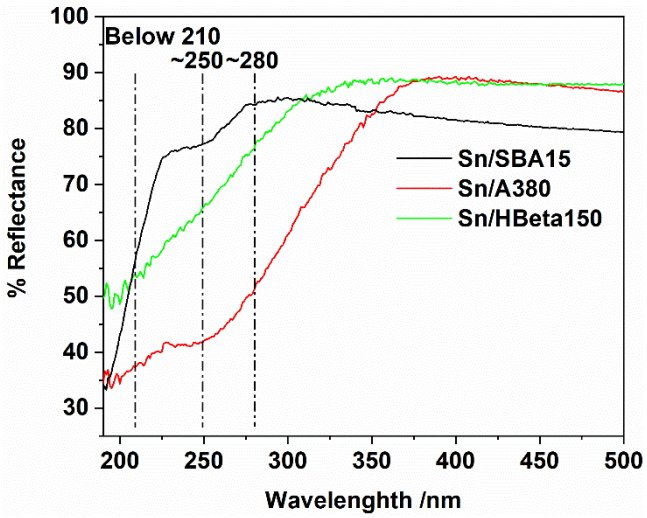

Fig. 5. comparison of DRUV-VIS spectra of silica supports containing 1 wt % Sn

These results show that the selective formation of tetrahedral Sn species on Sn/SBA15 catalyst was associated with its high selectivity towards fructose formation. We propose that the formation of tetrahedral Sn sites is correlated with the abundance of hydroxyl groups on the catalyst surface. The hydroxyl groups on silica surface can undergo condensation to form Si-O-Sn bonds under the acidic condition during catalyst preparation as shown in Scheme 1 [44]. SBA15 has higher abundance of surface hydroxyl groups in comparison to HBeta150 and A380 (Fig. S4). The large number of -OH present in SBA15 would facilitate high dispersion of Sn. Large pores of SBA15 would also prevent formation of tetrahedral closed Sn sites that are not active for this reaction.

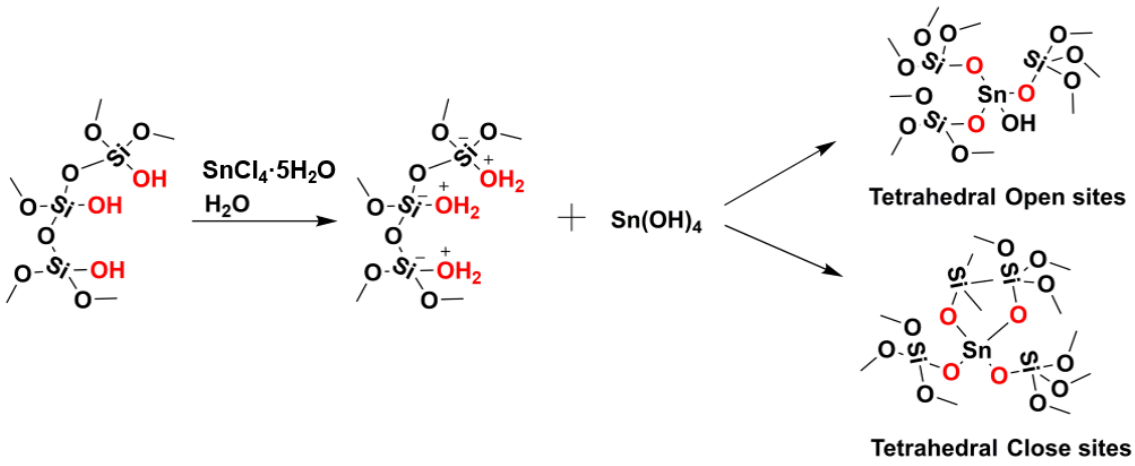

Scheme 1. Pathway for the formation of tetrahedral Sn sites the surface of SBA15. The -OH groups in red color are the surface hydroxyl groups (silanol) of SBA15.

Fig. S2 shows the XPS spectra of the O1s region for silica supported Sn catalysts samples. The prominent peak for oxygen atoms at 533.2 eV was assigned to the oxygen in Si-O-Si framework.[45] Another peak at 534.5 eV was observed that was assigned to oxygen in the surface hydroxyl groups. A small peak was observed near 531 eV for all silica containing supports. This peak was attributed to the formation of Si-O-M (M = metal) bond [46–49]. For Sn/HBeta150 this peak was prominent owing to the presence of Si-O-Al bonds in the zeolite framework. For Sn catalysts with SBA15 as support this peak appeared at 531.4 eV. In case of Sn/SBA15, the ratio of peak area for oxygen from Si-OH and Si-O-Sn bonds was 4.8: 1. Whereas for 3 wt % Sn/SBA15 the same ratio was 4.7: 1 suggesting similar density of Si-O-Sn bonds despite higher loading. Therefore, we concluded

that the formation of tetrahedral Sn species on the surface of catalyst is limited by the extent of surface hydroxyl groups present.

Finally, we performed high resolution microscopy of Sn/SBA15 to observe presence of Sn species. HR-TEM did not resolve any visible Sn particles on the SBA15 surface (Fig. S3). STEM image of Sn/SBA15 (Fig. 6) revealed small contrasting dots of size less than 0.3 nm presumed to be small Sn clusters or atomically dispersed Sn species. Elemental mapping of Si and Sn showed uniform distribution of Sn over the SBA15 surface which further concluded that highly dispersed Sn species present in tetrahedral geometry were the active sites. The corresponding EDS spectra for this region is shown in Fig. S6.

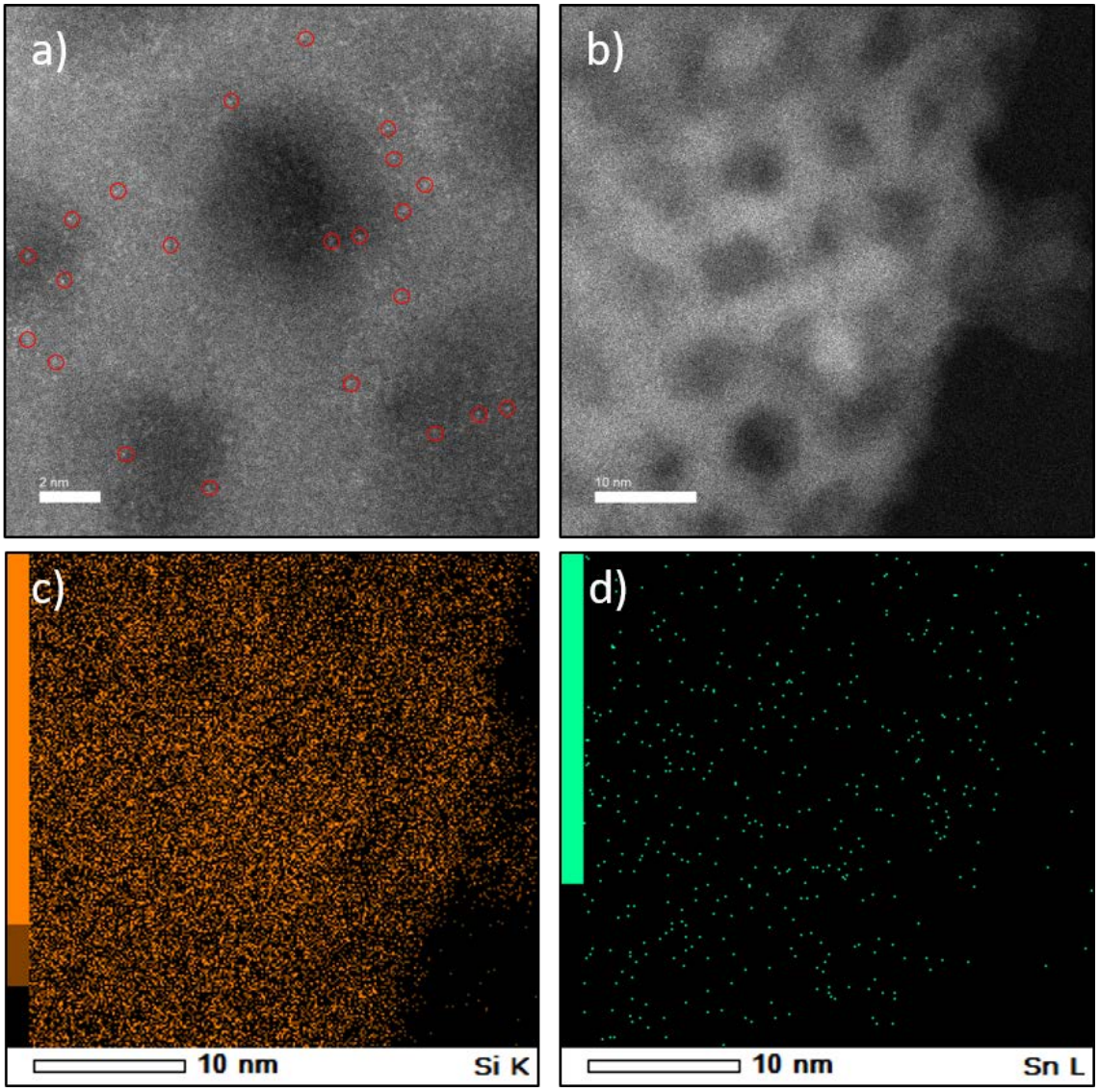

Fig. 6. a) STEM image of Sn/SBA15, circles highlight the particles presumed to the Sn species. b) STEM image of area of Sn/SBA15 used for elemental mapping. c) and d) elemental mapping of Si and Sn, respectively.

Pyridine was used as basic probe molecule, monitored by FTIR spectroscopy, to study the nature and strength of acid sites present in the catalysts. Sn/SBA15 showed a strong band at 1452 cm^{-1} [1] (Fig. 7a), which corresponds to interaction of basic pyridine molecule with Lewis acidic Sn centres [50–52]**.** The band at 1491 cm^{-1} can be ascribed to presence of both Lewis and Brønsted acidic centres. The silanol groups of SBA15 supports can act as weak Brønsted sites and contribute towards this peak. 3Sn/SBA15 and 5Sn/SBA15 catalysts also showed similar bands. However, the relative intensity for band at 1452 cm^{-1} for these catalysts was lower than that for Sn/SBA15 catalyst after desorption at 150 °C. Therefore, the strength of Lewis acid sites decreased with increasing Sn loading, which correlates with their catalytic performance. The spectra for Sn/HBeta150 catalyst exhibited both strong Brønsted acidity and Lewis acidity (the intense bands at 1491 cm^{-1} and 1546 cm^{-1}) as expected. Strength of Lewis acid sites in Sn/HBeta150 was similar to Sn/SBA15 as evidenced from similar peak intensity after 25 min evacuation under 0.03 torr pressure and desorption at 150 °C.

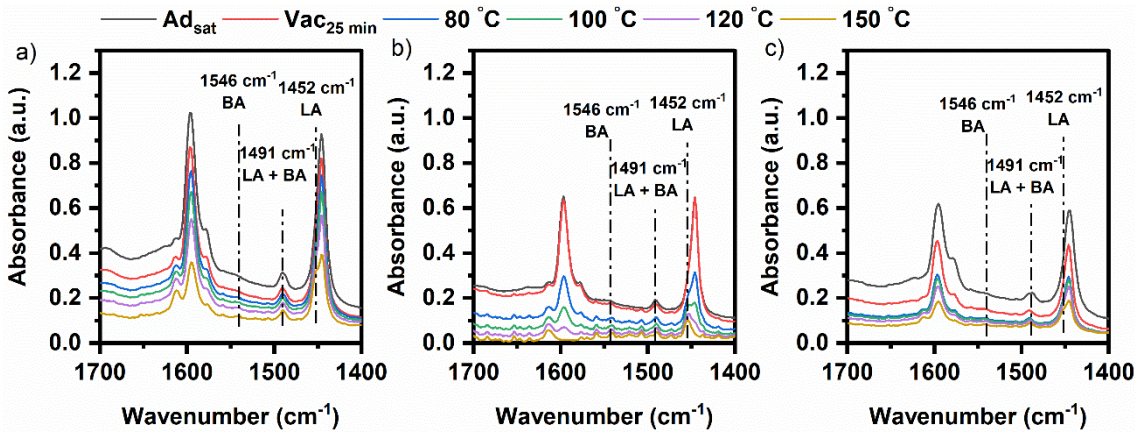

Fig. 7. IR spectra of adsorbed pyridine species over different catalysts. a) Sn/SBA15, b) 3Sn/SBA15, c) 5Sn/SBA15. Intensity of all the spectra are subtracted from that of corresponding samples before adsorption. The spectra were recorded at saturation adsorption condition (Ad_{sat}), after 25 min of evacuation at 0.03 torr ($Vac_{25\ min}$) and after desorption at various temperatures.

3.3 Isotopic labelling study

The presence of highly dispersed tetrahedral Sn sites would promote the glucose isomerization to proceed through the intramolecular hydride transfer mechanism, in which the proton

attached to the C2 carbon is transferred to the C1 atom (Scheme 2). In order to ascertain whether the glucose isomerization over Sn/SBA15 catalyst occurs *via* this mechanism, we performed an isotopic tracer study. D-glucose-2-d was used as the reactant instead of normal D-glucose and ^{2}H NMR spectroscopy of the product mixture was performed to detect the presence of deuterium (Fig. 8). The ^{2}H NMR spectrum of D-glucose-2-d standard showed two peaks centered at 3.49 and 3.27 ppm corresponding to ^{2}H at C2 position of the α and β anomers of glucose. After reaction, a new peak at 3.65 ppm corresponding to ^{2}H at C1 position of fructose appeared [14]. The presence of this peak confirmed the hydride transfer from C2 to C1 position, leading to the conclusion that glucose isomerization progressed through the Lewis acid catalyzed pathway over tetrahedral Sn sites.

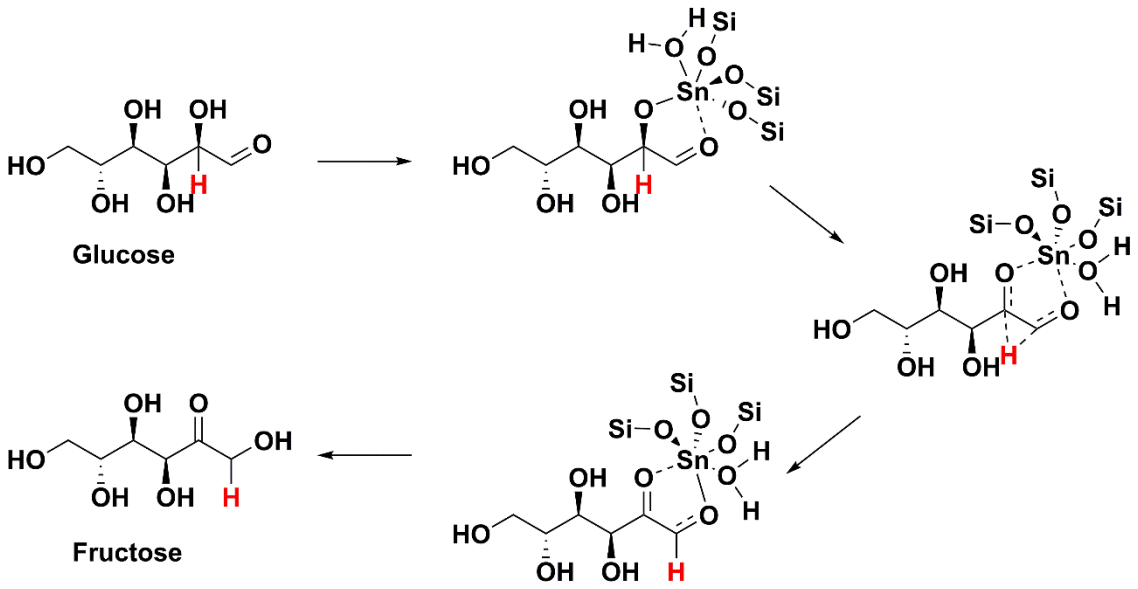

Scheme 2. Mechanism showing hydride transfer from C2 carbon of glucose to C1 carbon in fructose during isomerization over Lewis acidic Sn sites.

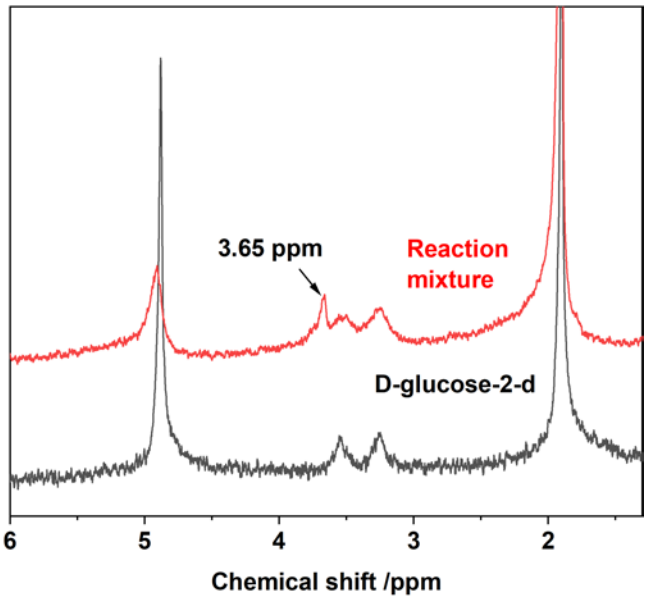

Fig. 8. ^{2}H NMR spectrum of reaction mixture, where D-glucose-2-d is taken as reactant. The reaction mixture is diluted with water and sodium acetate-d_3 was used as internal standard. The spectrum for D-glucose-2-d is also shown for reference. Reaction conditions: D-glucose-2-d 10 mg, Sn/SBA15 10 mg, 2mL ethanol 90 °C temperature, 2 h reaction time.

3.4 Recyclability study

Finally, we tested the reusability of Sn/SBA15 catalyst for glucose isomerization (Fig. 9). The recyclability test was done at 30 min of reaction time to keep the conversion below equilibrium. After each run the catalyst was washed with fresh ethanol and reused. The selectivity of fructose in the second cycle was the same as that for the fresh catalyst (99 %), although the glucose conversion dropped from 32% to 29%. In the third cycle the selectivity dropped to 78 % indicating deactivation of the catalyst. Deposition of small amount of humin might be attributed to the poor activity of catalyst. The catalyst was calcined again at 500 °C for 2 h after the third cycle, which regenerated the catalyst and the selectivity increased to 91 % with 32 % glucose conversion. To investigate weather Sn species leached into the reaction mixture, we carried out a reaction with Sn/SBA15 catalyst for 15 minutes, which produced 11 % fructose with 12 % glucose conversion. Then the catalyst was filtered and the filtrate was allowed to react further. No change was observed in either the glucose conversion or the fructose yield under this condition. Furthermore, Sn species were not detected in the EDX analysis of the reaction mixture. These results confirmed that leaching of Sn did not occur and the isomerization

reaction was heterogeneously catalyzed.

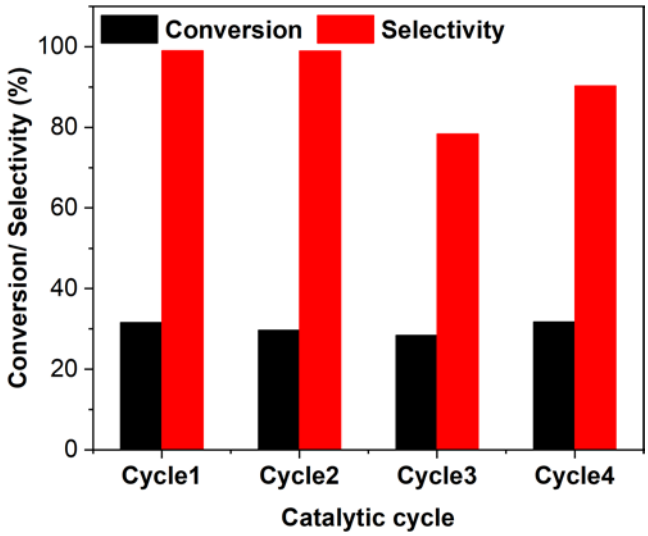

Fig. 9. Recyclability test of 1 wt. % Sn/SBA15. Reaction conditions: 90 mg glucose, 90 mg catalyst, 7 mL ethanol, 90 °C, 30 minutes.

4. Conclusion

We explored the formation of Lewis acidic tetrahedral Sn sites on the surface of oxides for isomerization of glucose to fructose. Silica based supports performed better than other oxides in catalytic isomerization when loaded with 1 wt. % Sn. Diffused reflectance UV-vis analysis showed a preference for formation of tetrahedral Sn sites instead of hexacoordinated SnO_2 over SBA15 support, which showed the best selectivity for fructose. The activity of SBA15 was attributed to the formation of Si-O-Sn bonds owing to high -OH density over SBA15. Increasing Sn loading beyond 1 wt. % over SBA15 also caused SnO_2 formation, which reduced selectivity. O1s XPS spectra for catalysts confirmed that increasing loading of Sn does not cause formation of new Si-O-Sn bonds, which is required for increasing number of tetrahedral Sn sites. Sn/SBA15 (1 wt. % Sn) showed high selectivity of 93 % with 57 % fructose yield after 2 h of reaction in the presence of ethanol. The reaction mechanism was confirmed to proceed through a 1,2-hydride shift by tracing the ^{2}H isotope in D-glucose-2-d, which indicated the Lewis acidic tetrahedral Sn sites as active sites in the reaction. The catalyst showed a decrease in activity after three cycles but removal of deposited organic compounds by calcination restored the activity.

5. Acknowledgement

A part of this work was supported by Hokkaido University microstructural characterization platform as a program of “nanotechnology Platform” of Ministry of Education, Culture, Sports, Science and Technology (MEXT), Japan.

6. References

[1] Y. Yang, C.W. Hu, M.M. Abu-Omar, Green Chem. 14 (2012) 509–513.

[2] D. Ding, J. Wang, J. Xi, X. Liu, G. Lu, Y. Wang, Green Chem. 16 (2014) 3846–3853.

[3] H. Kobayashi, A. Fukuoka, Green Chem. 15 (2013) 1740–1763.

[4] G. Yang, E.A. Pidko, E.J.M. Hensen, ChemSusChem. 6 (2013) 1688–1696.

[5] J.J. Pacheco, M.E. Davis, Proc. Natl. Acad. Sci. 111 (2014) 8363–8367.

[6] M. Kim, Y. Su, T. Aoshima, A. Fukuoka, E.J.M. Hensen, K. Nakajima, ACS Catal. 9 (2019) 4277–4285.

[7] J.P. Casey, I. Elkhart, Starch - Stärke. 29 (1977) 196–204.

[8] J. Jokela, O. Pastinen, M. Leisola, Enzyme Microb. Technol. 31 (2002) 67–76.

[9] I.A. Rose, E.L. O’Connell, R.P. Mortlock, BBA - Enzymol. 178 (1969) 376–379.

[10] K.N. Allen, A. Lavie, G.K. Farber, A. Glasfeld, G.A. Petsko, D. Ringe, Biochemistry. 33 (1994) 1481–1487.

[11] K.N. Allen, A. Lavie, A. Glasfeld, T.N. Tanada, D.P. Gerrity, S.C. Carlson, G.K. Farber, G.A. Petsko, D. Ringe, Biochemistry. 33 (1994) 1488–1494.

[12] A.Y. Kovalevsky, L. Hanson, S.Z. Fisher, M. Mustyakimov, S.A. Mason, V. Trevor Forsyth, M.P. Blakeley, D.A. Keen, T. Wagner, H.L. Carrell, A.K. Katz, J.P. Glusker, P. Langan, Structure. 18 (2010) 688–699.

[13] Y. Román-Leshkov, M. Moliner, J.A. Labinger, M.E. Davis, Angew. Chem., Int. Ed. 49 (2010) 8954–8957.

[14] M. Yabushita, N. Shibayama, K. Nakajima, A. Fukuoka, ACS Catal. 9 (2019) 2101–2109.

[15] J. Xu, K. Li, L. Zhang, H. Li, T. Wang, J. Biobased Mater. Bioenergy. 13 (2019) 739–747.

[16] X. Zhang, H. Li, X.X. Li, Y. Liu, X.X. Li, J. Guan, J. Long, ACS Sustain. Chem. Eng. 7 (2019)

13247–13256.

[17] R.O.L. Souza, D.P. Fabiano, C. Feche, F. Rataboul, D. Cardoso, N. Essayem, Catal. Today. 195 (2012) 114–119.

[18] R. Otomo, M. Fujimoto, M. Nagao, Y.K.-M. Catalysis, U. 2019, Mol. Catal. 475 (2019).

[19] N. Deshpande, E.H. Cho, A.P. Spanos, L.C. Lin, N.A. Brunelli, J. Catal. (2019) 119–127.

[20] N. Zhang, X.G. Meng, Y.Y. Wu, H.J. Song, H. Huang, F. Wang, J. Lv, ChemCatChem. 11 (2019) 2355–2361.

[21] L. Zhang, B. Deng, N. Li, H. Zhong, Bioresour. Bioprocess. 6 (2019).

[22] A. Corma, M.E. Domine, L. Nemeth, S. Valencia, J. Am. Chem. Soc. 124 (2002) 3194–3195.

[23] M. Moliner, Y. Román-Leshkov, M.E. Davis, Proc. Natl. Acad. Sci. 107 (2010) 6164–6168.

[24] R. Bermejo-Deval, R.S. Assary, E. Nikolla, M. Moliner, Y. Román-Leshkov, S.J. Hwang, A. Palsdottir, D. Silverman, R.F. Lobo, L.A. Curtiss, M.E. Davis, Proc. Natl. Acad. Sci. 109 (2012) 9727–9732.

[25] E. Nikolla, Y. Román-Leshkov, M. Moliner, M.E. Davis, ACS Catal. 1 (2011) 408–410.

[26] R. Bermejo-Deval, R. Gounder, M.E. Davis, ACS Catal. 2 (2012) 2705–2713.

[27] C.M. Lew, N. Rajabbeigi, M. Tsapatsis, Microporous Mesoporous Mater. 153 (2012) 55–58.

[28] Y.P. Li, M. Head-Gordon, A.T. Bell, ACS Catal. 4 (2014) 1537–1545.

[29] J.P. Lorenti, E. Scolari, E.M. Albuquerque, M.A. Fraga, J.M.R. Gallo, Appl. Catal. A Gen. 581 (2019) 37–42.

[30] I. Nekoksová, N. Silková, J. Čejka, Stud. Surf. Sci. Catal. 158 (2005) 1589–1596.

[31] N. Jiang, J.-B. Koo, S.-C. Han, S.-E. Park, Res. Chem. Intermed. 34 (2008) 507–517.

[32] D. Zhao, J. Feng, Q. Huo, N. Melosh, G.H. Fredrickson, B.F. Chmelka, G.D. Stucky, Science. 279 (1998) 548–552.

[33] S. Brunauer, P.H. Emmett, E. Teller, J. Am. Chem. Soc. 60 (1938) 309–319.

[34] P.P. Upare, A. Chamas, J.H. Lee, J.C. Kim, S.K. Kwak, Y.K. Hwang, D.W. Hwang, ACS Catal. 10 (2020) 1388–1396.

[35] A. Osatiashtiani, A.F. Lee, M. Granollers, D.R. Brown, L. Olivi, G. Morales, J.A. Melero, K.

Wilson, ACS Catal. 5 (2015) 4345–4352.

[36] L. Qi, Y.F. Mui, S.W. Lo, M.Y. Lui, G.R. Akien, I.T. Horváth, ACS Catal. 4 (2014) 1470–1477.

[37] J.S. Kruger, V. Choudhary, V. Nikolakis, D.G. Vlachos, ACS Catal. 3 (2013) 1279–1291.

[38] H. Huang, C.A. Denard, R. Alamillo, A.J. Crisci, Y. Miao, J.A. Dumesic, S.L. Scott, H. Zhao, ACS Catal. 4 (2014) 2165–2168.

[39] J. Tang, L. Zhu, X. Fu, J. Dai, X. Guo, C. Hu, ACS Catal. 7 (2017) 256–266.

[40] N. Chiodini, A. Paleari, D. Dimartino, G. Spinolo, Appl. Phys. Lett. 81 (2002) 1702–1704.

[41] F. Gu, S.F. Wang, C.F. Song, M.K. Lü, Y.X. Qi, G.J. Zhou, D. Xu, D.R. Yuan, Chem. Phys. Lett. 372 (2003) 451–454.

[42] G. Pang, S. Chen, Y. Koltypin, A. Zaban, S. Feng, A. Gedanken, Nano Lett. 1 (2001) 723–726.

[43] M. Bhagwat, P. Shah, V. Ramaswamy, Mater. Lett. 57 (2003) 1604–1611.

[44] P. Shah, A. V. Ramaswamy, K. Lazar, V. Ramaswamy, Microporous Mesoporous Mater. 100 (2007) 210–226.

[45] P. Post, L. Wurlitzer, W. Maus-Friedrichs, A.P. Weber, Nanomaterials. 8 (2018) 1–19.

[46] N. Elizondo-Villarreal, R. Obregón-Guerra, M. García-Méndez, A.P. Sánchez-Espinoza, M.A. Alcorta-García, R.O. Torres-Barrera, V. Coello, V.M. Castaño, Rev. Adv. Mater. Sci. 47 (2016) 74–78.

[47] J. Zhang, L.R. Grabstanowicz, S. Gao, N.S. Hosmane, B. Huang, Y. Dai, D.J. Liu, T. Xu, Catal. Sci. Technol. 2 (2012) 390–399.

[48] X. Cui, C. Chen, S. Sun, D. Zhou, F. Ndayisenga, M. Huo, S. Zhu, L. Zhang, J.C. Crittenden, Water Res. 143 (2018) 136–145.

[49] H. Fu, X. Ding, C. Ren, W. Li, H. Wu, H. Yang, RSC Adv. 7 (2017) 16513–16523.

[50] E.P. Parry, J. Catal. 2 (1963) 371–379.

[51] M.M. Maronna, E.C. Kruissink, R.F. Parton, F. Soulimani, B.M. Weckhuysen, W.F. Hoelderich, Phys. Chem. Chem. Phys. 18 (2016) 22636–22646.

[52] W.N.P. Van Der Graaff, C.H.L. Tempelman, E.A. Pidko, E.J.M. Hensen, Catal. Sci. Technol. 7 (2017) 3151–3162.